Arrangement and dynamics of individual cyclodextrins on the surface of core-shell micelles

I.S. Vaskan[1*], V.A. Dimitreva[1,2], A.A. Piryazev[4], E.N.Subcheva[4], N.V. Bovin[1], A.B. Tuzikov[1], V.A. Oleinikov[1,2] and A.V. Zalygin[1,3*]

[1]*Shemyakin-Ovchinnikov Institute of Bioorganic Chemistry, Russian Academy of Sciences, Moscow, 117997, Russia*
[2]*National Research Nuclear University Moscow Engineering Physics Institute, Moscow, 115409, Russia*
[3]*Lebedev Physical Institute, Russian Academy of Sciences, Troitsk Branch, Troitsk, Moscow, 108840, Russia*
[4]*Sirius University of Science and Technology, 1 Olympic Ave, 354340, Sochi, Russian Federation*
Russian Federation
*Corresponding authors:
vaskan.ivan@inbox.ru (IV)
zalygin.anton@gmail.com (AZ)

Abstract
Efficient site-specific drug delivery systems (DDS) would require sophisticated surface structure to overcome challenges arising from currently inevitable interactions with components of complex biological environment. One way to endow nanoparticles (NPs) with the designed surface properties is to use excipients that enable appropriate multivalent surface modifications. In this respect, cyclodextrins (CDs) is a versatile building block that can be used to provide NPs various surface modifications as well as drug loading capacity by means of host-guest interactions. On the other hand, structural properties of CD-decorated NPs including localization, orientation, and mobility of individual CDs should be assessed for rational design of DDS and control over its surface properties. In this paper, we used combination of transmission electron microscopy (TEM), small-angle X-ray scattering (SAXS) and molecular dynamics(MD) to assess these structural and dynamical properties of α- and β-CD-decorated core-shell micelles based on NPs topography maps. Micelles self-assemble from function-spacer-lipid (FSL) constructs that are conjugates of CDs, phospholipid DOPE and hydrophylic *N*-carboxymethyloligoglycine spacer. It was found that most of CD residues lose their functionality because of their clustering and unfavorable orientation, that results in CD cavity becomes inaccessible for binding. Dynamics of NPs surface structure reveals that CDs have low mobility, due to their interactions with oligoglycine spacer that prone to form static shell. Reducing the density of CD and spacer by 5 times prevents clusterization suggesting optimal density of CD residues, but does not affect CDs orientations and mobility. These findings indicate that the functionality of CD residues depends on the type of spacer and CD and their junction, and simple conjugation may not be enough to properly orient CDs on the surface. The combination of oligoglycine spacer with CD can be used as an excipient that turn hydrophobic core into stable multivalent scaffold to which various functional compounds can be attached through guest-host interactions. Obtained insights could be useful in development of CD-based NPs surface modifications towards rational design of smart next generation drug delivery systems.

Keywords: cyclodextrins, drug delivery, rational design, nanoparticles, surface structure, function-spacer-lipid constructs

Introduction

Nanotechnology advances resulted in emergence of numerous nanoparticle-based drug delivery systems (reviewed in [1]). However, current nanocarriers show low efficiency and severe side effects [2]. This is explained by the fact that after introduction to biological environment (i.e. bloodstream), nanoparticle encounter numerous obstacles on their way to target site, which conventional nanoparticles relying only on EPR (Enhanced Permeability and Retention) effect unable to overcome. These obstacles originate from molecular interactions at nano-bio interface indicating that surface structure and dynamics is a key factor predetermining the biological fate of nanoparticles [3]. Recent research is focused on studying nanoparticles with various surface chemistries endowing it with such properties as stimuli-responsiveness[4], low protein adsorbtion[5-7] and enhanced targeting[8]. The results of such studies suggest that to increase efficiency, nanoparticles must have a complex multivalent surface. Therefore, the ability to impart various properties to the surface of nanoparticles is important for exploring and exploiting ways to increase their efficiency. In this regard, cyclodextrins are a versatile tool for various surface modifications due to their unique physico-chemical properties[9].

Cyclodextrins are natural cyclic oligosaccharides composed of a(1-4)-linked glucose units produced by enzymatic degradation of starch. The most common CDs have six, seven or eight glucose units and named α-CD, β-CD, γ-CD respectively. Glucose units are closed in a cycle in such a way that all primary hydroxyls are on one rim of the cycle, while secondary hydroxyls occupy the opposite rim. Such configuration results in the truncated cone three-dimensional structure of CDs with hydrophilic exterior and hydrophobic interior. Due to their natural origin, CDs are non-toxic and non-immunogenic, and the presence of apolar cavity which can host small hydrophobic molecules provides wide opportunities for grafting various chemical compounds by means of host-guest interactions[10]. Due to these remarkable properties, CDs have gained much attention in biomaterials research, resulted in numerous CD-based nanomaterials such as polymeric NPs[11], hydrogels[12], nanosponges[13], functional glyconanomaterials[14], CD-peptide conjugates[15] that have been proposed for biomedical applications. In the field of drug delivery, they are used for nucleic acid delivery[16], to impart stimuli responsivness[17], for drug activity enhancement[18]. In recent works, CD are studied as toxin adsorbents[19], for macrophage-targeted delivery[20], for chiral recognition[21]. These results indicate great potential for CD to improve the efficiency of delivery systems. However, the main challenge in developing delivery systems is the lack of knowledge about behavior of such systems at the nanoscale[22]. Rational design of therapeutic nanoparticles requires precise control over the surface properties at the molecular level, especially when these properties are achieved through interactions between multiple components.

In this paper we study structure and dynamics of nanoparticles self-assembled from function-spacer-lipid constructs(FSL)[23], which are conjugates of phospholipid DOPE, hydrophilic spacer and functionalized with α- or β-CD. Of particular interest is the structure and dynamics of the surface of nanoparticles, as well as the molecular properties of individual cyclodextrins such as localization, orientation, mobility. This work is aimed at deepening our understanding of bihavior of CD on the surface of funtionalized NPs and the influence of the spacer on it towards rational design of drug delivery systems.

Materials and Methods.

Materials.

All salts, solvents, lipids and other chemicals were from Sigma (St.Louis, USA). CD-$(CMG)_4$-DOPE constructs were synthesized (Scheme 1) from monoamino derivatives of alpha- and beta-cyclodextrins and H-$(MCMG)_4$-OH amino acid, which after hydrolysis of methyl ester groups forms a hydrophilic spacer $(CMG)_4$.

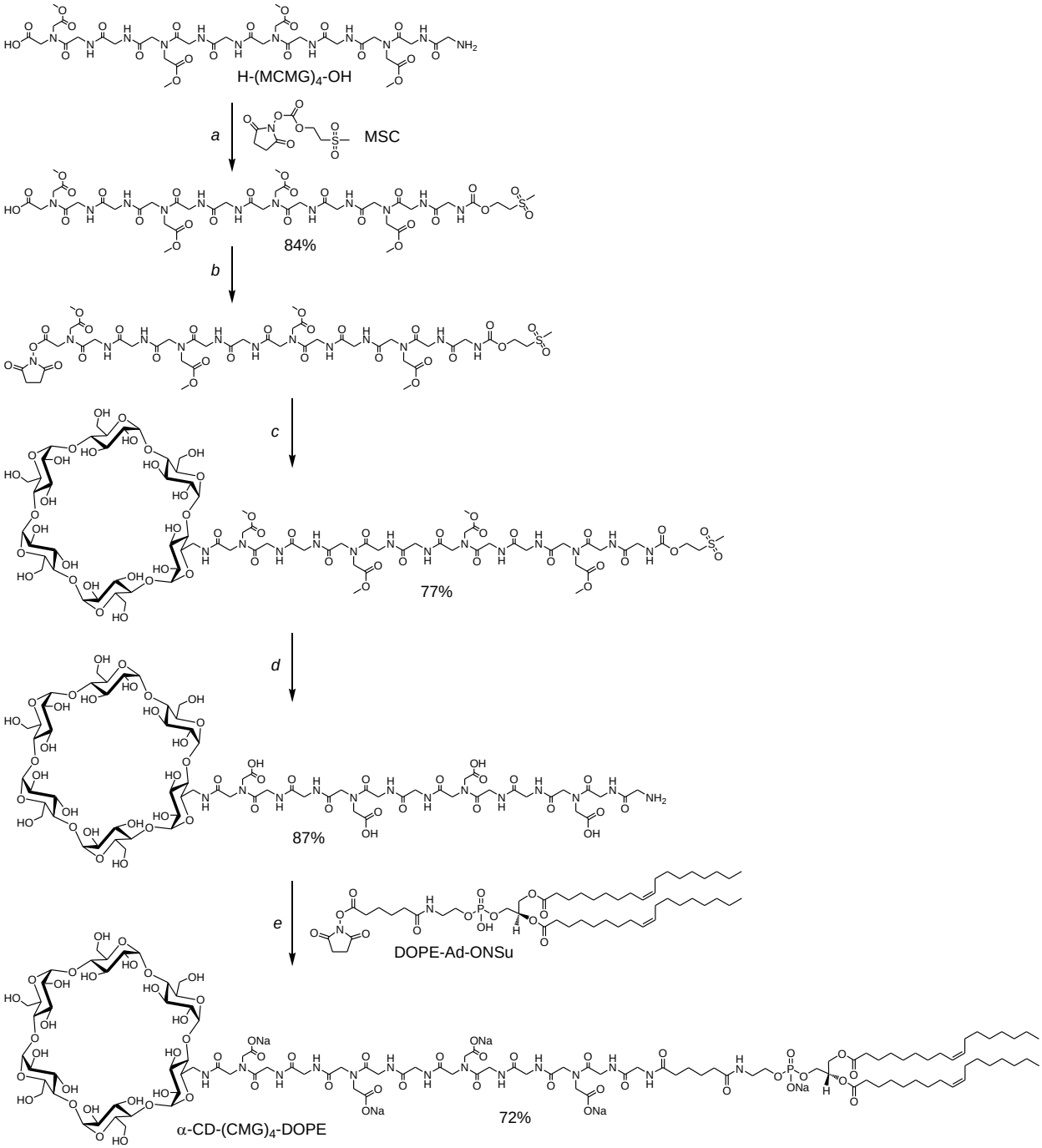

Scheme 1. Synthesis of α-CD-$(CMG)_4$-DOPE. Reagents and conditions: (a) DMF, Et_3N, 2 h / r.t., isolation on Sephadex LH-20 in MeCN/H_2O 1:1; (b) DMF, N-hydroxysuccinimide, N,N-dicyclohexylcarbodiimide, 20 h / r.t.; (c) α-cyclodextrin monoamine, DMF, Et_3N, 1 h / r.t., isolation on Sephadex LH-20 in MeCN/H_2O 1:1; (d) H_2O, Et_3N (2% by volume), 2 h / r.t., isolation on Sephadex LH-20 in MeCN/H_2O 1:1; (e) 2-propanol/water 3:2, $NaHCO_3$, DOPE-Ad-ONSu in 1,2-dichloroethane, 1 h / r.t., isolation on reverse phase C_{18} MeOH/water 1:2 → MeOH/water 2:1 → MeOH/water 2:1 + 5% $CHCl_3$.

The introduction of the methylsulfonylethoxycarbonyl protective group (MSC) to amino group of H-$(MCMG)_4$-OH, activation of carboxyl, conjugation with the monoamino derivative of cyclodextrin, removal of protective groups and conjugation with the lipid block DOPE-Ad-ONSu gave the desired product (Scheme 1).

H-$(MCMG)_4$-OH amino acid is courtesy of A.A. Formanovsky (Shemyakin-Ovchinnikov Institute of Bioorganic Chemistry of the Russian Academy of Sciences). Aminoderivatives of cyclodextrins 6-monoamino-6-monodeoxy-α-cyclodextrin and 6-monoamino-6-monodeoxy-β-cyclodextrin were from AraChem (Netherlands). 2-(Methylsulfonyl)-ethyl-*N*-succinimidyl carbonate (MSC) was from Fluka, *N*-hydroxysuccinimide and *N*,*N*'-dicyclohexylcarbodiimide were from Merck, Sephadex LH-20 was from Sigma-Aldrich. DOPE-Ad-ONSu was synthesized as described in [23].

α-CD-(CMG)$_4$-DOPE

TLC: R_f = 0.32 ($CHCl_3$/MeOH/H_2O 3:6:1).

^{1}H NMR (CD_3OD/D_2O 1:1, 303 K, 700 MHz) δ

5.374 (m, 4H; CH=CH), 5.291 (m, 1H; 2-CH of glycerol), 5.043 (m, 6H; 6 H-1 of Gluc), 4.753 (s, HOD), 4.474 (dd, *J* = 12.2, 2.5 Hz, 1H; 1-CH of glycerol), 4.238 (dd, *J* = 12.2, 7.5 Hz, 1H; 1-CH` of glycerol), 4.280-3.741 (m, 63H; 24H of Gluc, 32H of CMG, 7H of DOPE), 3.603 (m, 10H of Gluc), 3.440 (m, 2H; CH_2N), 3.344 (p, *J* = 1.7 Hz; CD_2HOD methanol), 2.368 (m, 6H; 3 CH_2CO), 2.290 (m, 2H; CH_2CO), 2.032 (m, 8H; 2 $CH_2C{=}CCH_2$), 1.633 (m, 8H; 4 CH_2CH_2CO), 1.321 (m, 40H; 20 CH_2 of Oleoyl), 0.912 (t, *J* = 7.1 Hz, 6H; 2 CH_3) ppm.

MALDI-TOF MS: found m/z 2786.218; calc. for $C_{115}H_{188}N_{14}O_{59}PNa_2$ $[M-H+2Na]^+$ 2786.167.

β-CD-(CMG)$_4$-DOPE was obtained similarly α-CD-(CMG)$_4$-DOPE, the yields are similar.

TLC: R_f = 0.34 ($CHCl_3$/MeOH/H_2O 3:6:1).

^{1}H NMR (CD_3OD/D_2O 1:1, 303 K, 700 MHz) δ

5.375 (m, 4H; CH=CH), 5.291 (m, 1H; 2-CH of glycerol), 5.056 (m, 7H; 7 H-1 of Gluc), 4.762 (s, HOD), 4.472 (dd, *J* = 12.2, 2.5 Hz, 1H; 1-CH of glycerol), 4.239 (dd, *J* = 12.2, 7.5 Hz, 1H; 1-CH` of glycerol), 4.284-3.735 (m, 67H; 28H of Gluc, 32H of CMG, 7H of DOPE), 3.611 (m, 12H of Gluc), 3.439 (m, 2H; CH_2N), 3.344 (p, *J* = 1.7 Hz; CD_2HOD methanol), 2.374 (m, 6H; 3 CH_2CO), 2.292 (m, 2H; CH_2CO), 2.042 (m, 8H; 2 $CH_2C{=}CCH_2$), 1.646 (m, 8H; 4 CH_2CH_2CO), 1.336 (m, 40H; 20 CH_2 of Oleoyl), 0.915 (t, *J* = 7.1 Hz, 6H; 2 CH_3) ppm.

MALDI-TOF MS: found m/z 2948.268; calc. for $C_{121}H_{198}N_{14}O_{64}PNa_2$ $[M-H+2Na]^+$ 2948.220.

Samples were prepared by dissolving weighed portions of α-CD-(CMG)$_4$-DOPE, β-CD-(CMG)$_4$-DOPE in PBS buffer. Chemical structures of α-CD-(CMG)$_4$-DOPE, β-CD-(CMG)$_4$-DOPE monomers shown in Figure 1. For TEM and SAXS studies concentration of all samples was 2 mM.

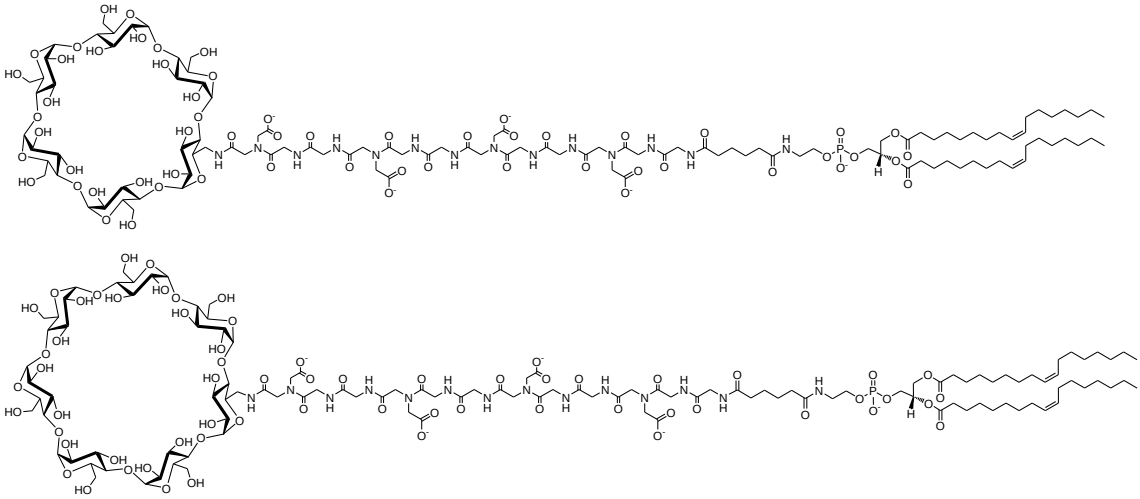

Figure 1. Chemical structure of studied molecules: α-CD-(CMG)$_4$-DOPE (top), β-CD-(CMG)$_4$-DOPE (bottom). DOPE is 1,2-O-dioleoyl-*sn*-glycero-3-phosphoethanolamine; (CMG)$_4$ is repeating glycyl-glycyl-N-carboxymethylglycyl motif.

Critical micelle concentration (CMC) measurements.

The critical micelle concentration (CMC) was determined by the fluorescence probe technique using pyrene as a fluorescence probe. The samples for CMC measurements were prepared by serial dilution of stock sample PBS solution with concentration varied from 250 to 0.025 μM. Pyrene concentration (0.2 μM) was kept constant during measurements. The pyrene fluorescence spectra were recorded using a RF-5301PC spectrofluorophotometer (Shimadzu, Japan), λex= 334 nm, λem= 350–450 nm, slidwidth(ex) = slidwidth(em) = 3 nm, step width 1 nm. The sample concentrations were plotted against the I_{385}/I_{375} peaks ratio of the fluorescence intensity and subsequently fitted with a logistic function, whereby the CMC value of each sample was determined.

Transmission electron microscopy

Sample preparation: solutions of the studied samples were vortexed for 30 seconds, then applied to the surface of a 300 mesh copper grid with a carbon/forvar coating (EMCN, China) in a volume of 2.5 μl and incubated for 1 minute. Excess liquid was drawn off with filter paper. Contrasting was performed with a 1% aqueous solution of uranyl acetate for 1 minute. The grids were dried at room temperature in air.
The image capture was carried out on a Crossbeam550 scanning electron microscope with a detector for transmission electron microscopy (Carl Zeiss, Germany) at an accelerating voltage of 30 kV.

Small Angle X-ray Scattering (SAXS)
SAXS experiments were performed using XeuSS 3.0 WAXS/SAXS (Xenocs, France) machine with GeniX3D generator (λ = 1.54 Å), producing beam with 300x300 μm size. Pilatus300k detector was used for data collecting, and sample–detector distance was 1.3m. The minimum projection method for a series of images was used to reduce background noise (12 frames with 1h exposition). Norm wave vector s (s = 2sinθ/λ, where θ is Bragg angle) was calibrated via several orders of AgBe. The data were corrected for the solvent scattering and processed using standard procedures with a program suit ATSAS [24].

SAXS and TEM measurements were supported by the Ministry of Science and Higher Education of the Russian Federation, (Agreement 075-10-2021-093).

Molecular dynamics simulation

Atomistic molecular dynamic was carried out using GROMACS package version 2024[25]. Starting structure consisted of spherically arranged monomers (pre-micelle) solvated in water with salt concentration of 150 mM. Number of monomers(190) was chosen so that radius of gyration of simulated micelles(trajectory average) was consistent with experimental value derived from SAXS data. GROMOS 54A7 force field topologies for monomers were generated using Automated Topology Builder[26]. Pre-micelles were minimized with turned off non-bonded interactions in order to decouple overlapping atoms. Next, a short 60 ps simulated annealing stochastic dynamic run was performed to reach global minimum. After energy minimization and two 10 ps equilibration runs in NVT and NPT ensembles, 450 ns production run was performed using the NPT ensemble with periodic boundary conditions applied (P = 1 bar and T = 298 K). Non-bonded interactions were calculated using the cutoff distance of 1 nm. Long-range electrostatic interactions were calculated by the PME method and the MD integration time step was set to 1.6 fs. VMD1.9.3[27] was used for visualization. Fitting to experimental SAXS curve was performed using CRYSOL[28] program from ATSAS package. First 350 ns were omitted for equilibration and remaining 100 ns (1000 frames) were used for processing including trajectory rotational fit to remove displacement of atoms caused by nanoparticle rotation, root mean square deviation (RMSD) calculation for surface atoms, extraction of frames with minimal, average and maximal RMSD over trajectory and topography maps generation. Topography generation was performed similarly to previous work[29]. Briefly, lipid atoms were excluded from MD coordinates and GROMACS built-in tool was used for Connolly surface computation using algorithm [30] with probe radius of 1.42 A. Obtained surface was plotted in spherical coordinates.
Mixed micelles consisted of 152 DOPE lipids and 38 CD-$(CMG)_4$-DOPE conjugates were simulated with the same protocol, except for production run time was 200 ns and last 75 (750 frames) ns were taken for processing.

Results and Discussion
To make sure that CD-containing conjugates self-assemble into micellular nanoparticles, as a first step of the study we have determined critical micelle concentration(CMC). Results are shown in Figure 2.

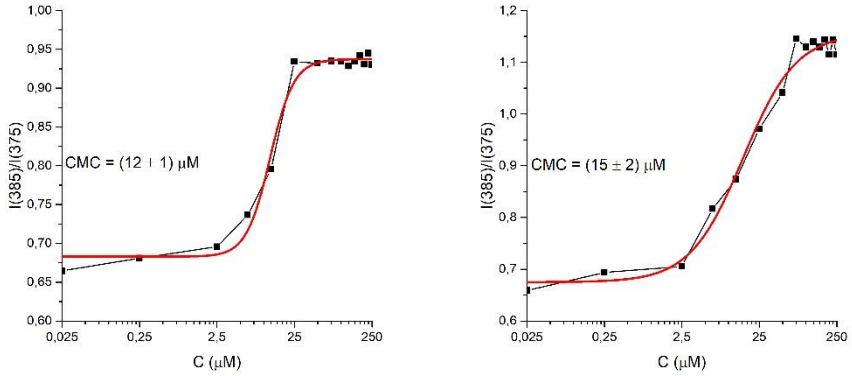

Figure 2. Critical micelle concentration(CMC) determination of α-CD-$(CMG)_4$-DOPE micelles (left), β-CD-$(CMG)_4$-DOPE micelles (right). Black: experimental data, red: logistic fit.

It can be seen that for both α-CD- and β-CD-containing conjugates CMC values is around 15 μM. These values indicate significantly higher stability of lipid-based micelles compared to their polymeric counterparts, which have CMC values around 5 mM. Next, we have applied transmission electron microscopy(TEM) to visually confirm micelles formation, and determine their sizes. Obtained images are shown in Figure 3.

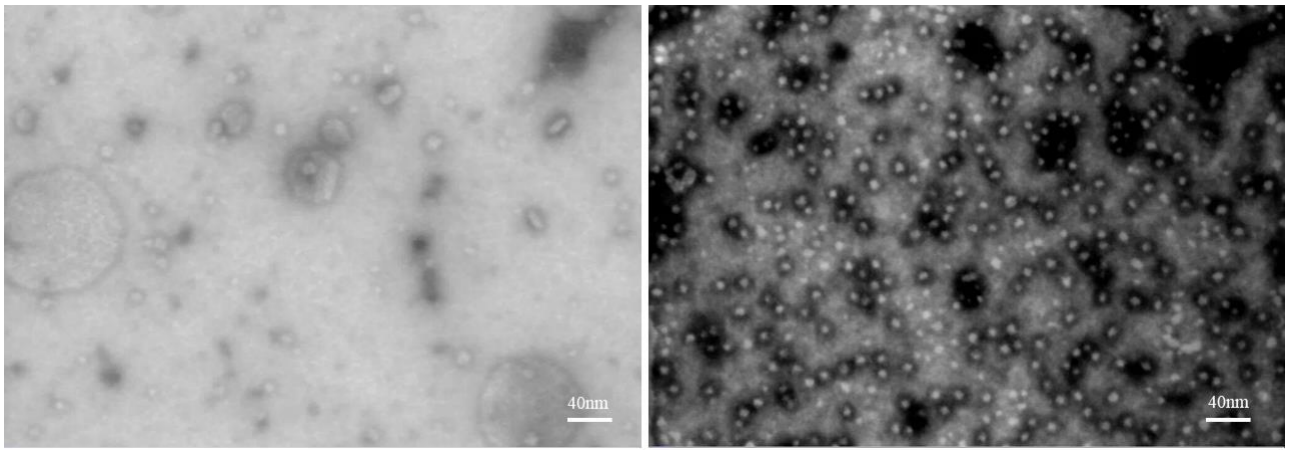

Figure 3. Transmission electron microscopy images of α-CD-CMG(4)lin-DOPE micelles (left) and β-CD-CMG(4)lin-DOPE micelles (right). Scale mark: 40 nm.

It can be seen that many round-shaped particles are formed. α-CD- and β-CD-bearing micelles show similar size of about 10-12 nm, which is in agreement with previous studies of similar conjugates [29,31]. To determine nanoparticle size and internal structure under physiological conditions, small-angle X-ray scattering (SAXS) technique was applied. Resulting SAXS curves shown in Figure 4.

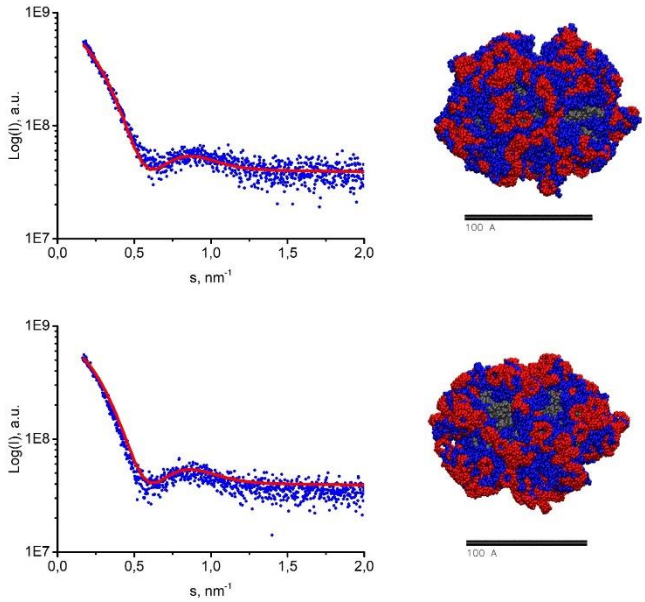

Figure 4. Small Angle X-ray Scattering (SAXS) data (blue dots), scattering profile derived from molecular dynamics simulations(red line), molecular dynamics nanoparticle snapshots for α-CD-$(CMG)_4$-DOPE micelles (top), β-CD-$(CMG)_4$-DOPE micelles (bottom). Nanoparticle color scheme: core in grey, CMG spacer in blue, cyclodextrins in red.

Such curves are typical for micellular nanoparticles. Radius of gyration(R_g) derived from these curves was found to be 5.2 nm and 5.4 nm for α-CD- and β-CD-bearing micelles, respectively, which is in agreement with TEM study. Another feature of the SAXS technique is that experimental data can be directly compared with curves from nanoparticle models obtained using molecular dynamics(MD) simulations. Thus, SAXS data can be used to validate MD models, which, in case of a good fit, allows one to study the structure of nanoparticles with the resolution of atomistic molecular dynamics. Figure 4 also shows fit of curve calculated from MD model (red line) to experimental data, with chi square (χ^2) values of 1.5 and 1.2 for α-CD- and β-CD-bearing micelles, respectively. Such χ^2 values indicate that simulated nanoparticles are consistent with nanoparticles in solution. Snapshots of simulated nanoparticles (trajectory average) are also shown in Figure 4. From these models it can be seen that micelles possess core-shell structure; hydrophobic core is almost completely covered by a hydrophilic spacer, with cyclodextrins located predominantly on the surface. With regard to the arrangement of cyclodextrins, two points that affect CDs functionality are noteworthy. First, it is evident that many cyclodextrins are located close to each other, which can lead to overlaps that prevent the binding of ligands by individual CDs. Second, cyclodextrins have different orientations relative to the external environment. To address these pints and study arrangement of cyclodextrins in more detail, we have generated and analyzed topography of micelles, shown in Figure 5.

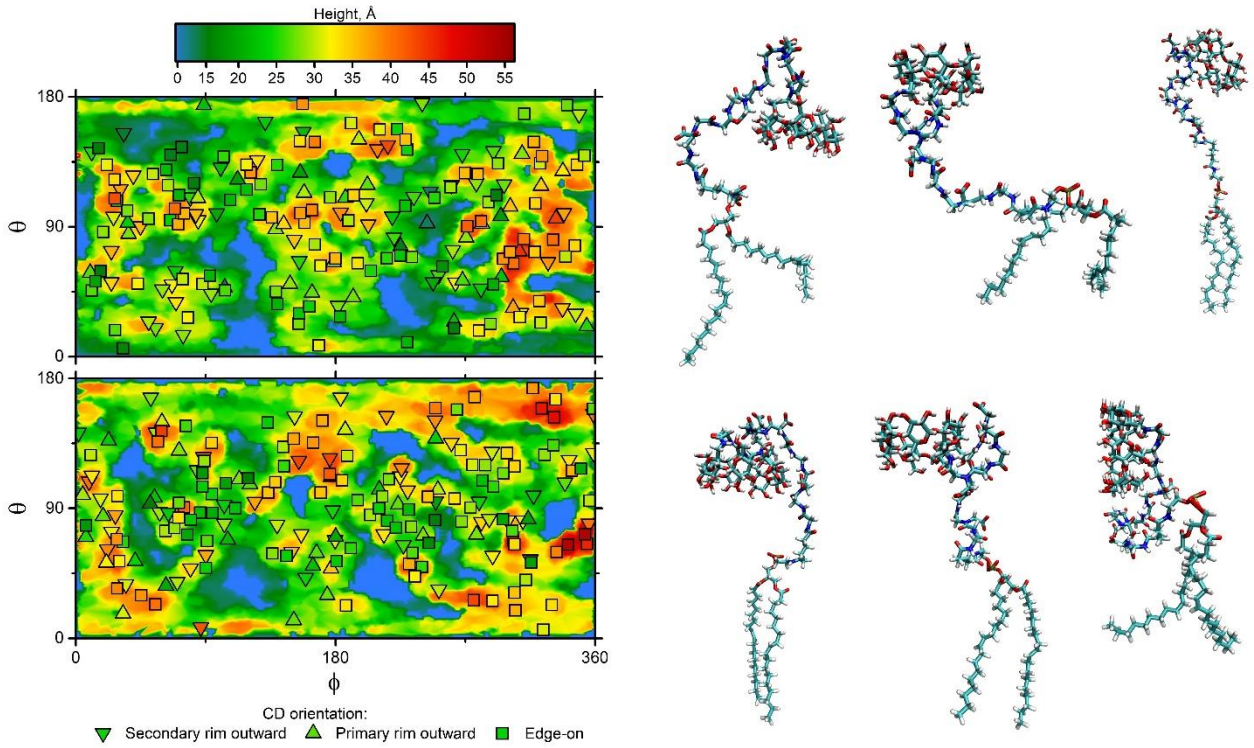

Figure 5. Molecular dynamics simulation results. Left to right: micelle topography map, preferred molecular conformations with primary rim outward CD orientation, secondary rim outward CD orientation, edge-on CD orientation for α-CD-$(CMG)_4$-DOPE micelles (top), β-CD-$(CMG)_4$-DOPE micelles (bottom). Positions of cyclodextrins center of geometry are marked with figures. Triangle corresponds to primary rim outward CD orientation, inverted triangle corresponds to secondary rim outward CD orientation and square corresponds edge-on CD orientation. Color of a figure corresponds to its height. Scale along the ϕ axis: 360° ≈ 35 nm at θ = 90°, for an arbitrary angle θ the scale increases as 35*sin(θ). Scale along the θ axis is constant: 180° ≈ 15 nm. Molecule color scheme: hydrogens are in white, carbons are in cyan, oxygens are in red, nitrogens are in blue, sulfurs are in yellow and phosphorus atoms are in tan.

Nanoparticles surface is plotted in spherical coordinates, heights over the core(shell thickness) are indicated by color. Cyclodextrin positions with three possible orientations are marked with geometrical figures. Triangle, inverted triangle and square correspond to secondary rim outward, primary rim outward and edge-on CD orientation, respectively. Monomers with these CD orientations are also shown in Figure 5. Topography maps enable assessment of each CD and identify those that retain their functionality. By comparing the colors of the figure and its surroundings, one can judge whether the given CD is on the surface or entangled by a spacer or other CD. It is clear that to retain the ability to bind ligands, cyclodextrin must be located on the surface, have secondary rim outward orientation and not overlap with other molecules. From topography maps it can be seen that only a small fraction of CD residues satisfy these conditions. We identify 41 and 45 functional CD residues (out of 190) for α-CD- and β-CD-bearing micelles, respectively. These functional CD residues are distributed throughout the surface of nanoparticle, which indicates that the presence of a CD residue in each monomer is not mandatory from a quantitative perspective. Next, we assess mobility of CD residues with appropriate orientation since the ability of CD to slightly shift its position towards ligand may increase the chance of binding event. To do this, we study the dynamics of nanoparticle topographies by comparing the extreme states between which the surface of the nanoparticles fluctuates, which corresponds to MD trajectory frames with minimal and maximal root mean square deviations(RMSD). Corresponding topographies are shown in Figure 6.

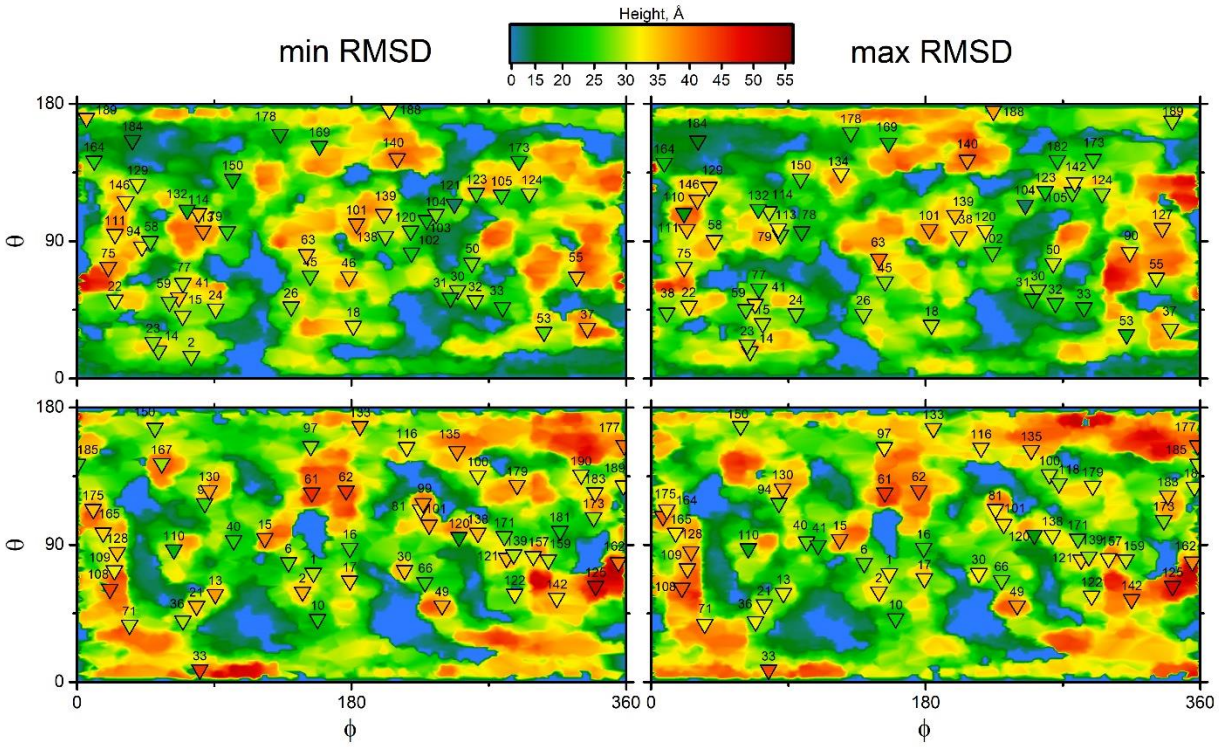

Figure 6. Dynamics of nanoparticle topography. Min RMSD(left) and max RMSD(right) surface structure for α-CD-$(CMG)_4$-DE micelles (top), β-CD-$(CMG)_4$-DE micelles (bottom). Positions of centers of geometry of cyclodextrins with secondary rim outward CD orientation are marked with inverted triangles. Marks are numbered to identify each CD and track its mobility. Scale along the ϕ axis: 360° ≈ 35 nm at θ = 90°, for an arbitrary angle θ the scale increases as 35*sin(θ). Scale along the θ axis is constant: 180° ≈ 15 nm.

The first thing to notice is that both for α-CD- and β-CD-bearing micelles possess static surface formed by a practically immobile shell. Most CD residues also stayed in the same position. However, there are several displaced CD residues which indicates their mobility. For α-CD-bearing micelles these are residues 37, 55,58,79,104,120,189 (7 in total) and in case of β-CD-bearing micelles only residue 185 is mobile. Furthermore, some CD residues are able to change their orientation, which suggests that they also have some mobility. In case of α-CD-bearing micelles these are residues 2,38,46,78,90,94,110,121,127,134,142,182 (12 in total). β-CD residues with switched orientation are 41,99,118,164,167,181,190 (7 in total). Thus, α-CD residues demonstrate overall greater mobility than β-CD. A possible reason for the observed static nature of the surface and low mobility of CD residues may be the formation of hydrogen bonds. Indeed, calculation of hydrogen bonds reveal that there are 2084 and 3041 H-bonds between shell moieties of α-CD- and β-CD-bearing micelles, respectively, that stabilize surface structure.

To find out whether such dynamics of surface structure and CD orientation are a consequence of the high density of the shell and CDs, we simulated the self-assembly of mixed micelles in which only 20% of the total number of molecules have spacer and CD residues. Dynamics of corresponding nanoparticles topographies shown in Figure 7.

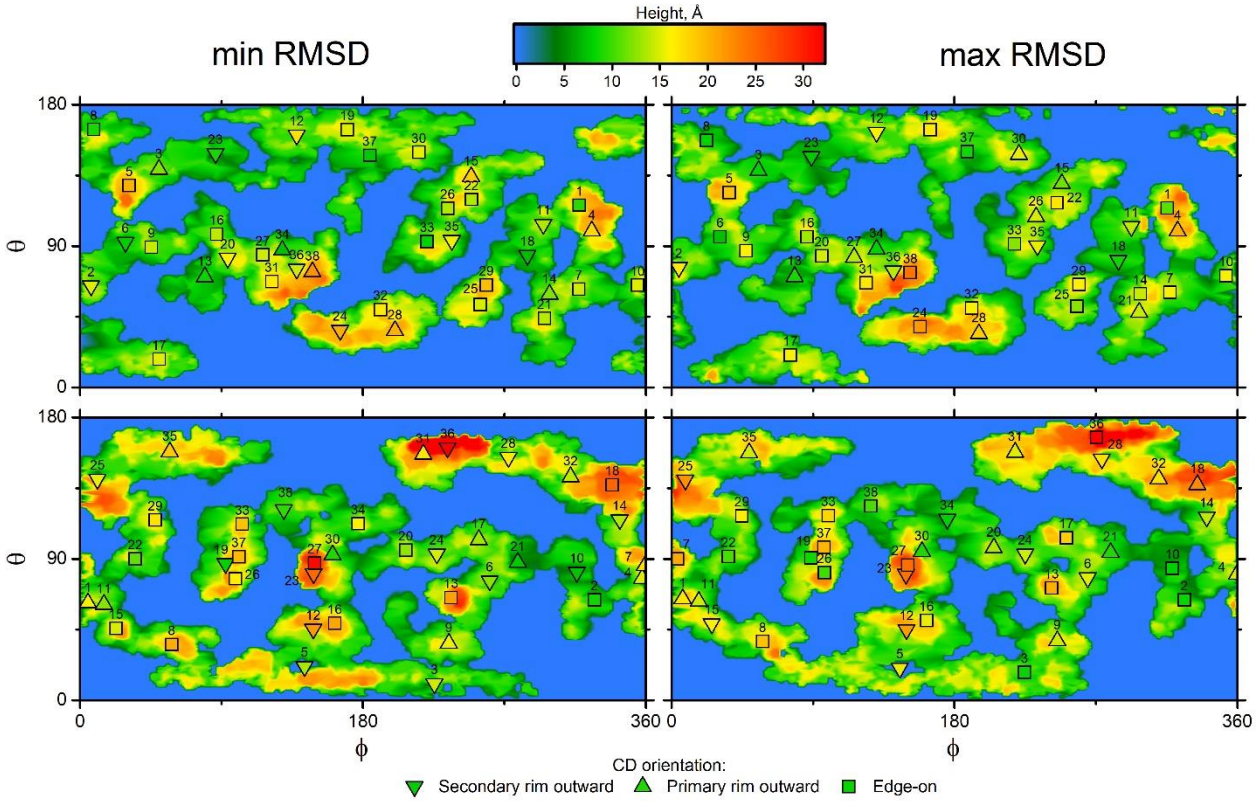

Figure 7. Dynamics of nanoparticle topography. Min RMSD(left) and max RMSD(right) surface structure for micelles composed of 152 DOPE lipids and 38 α-CD-(CMG)$_4$-DOPE conjugates (top), 152 DOPE lipids and 38 β-CD-CMG(4)lin-DOPE conjugates (bottom). Positions of cyclodextrins center of geometry are marked with figures. Triangle corresponds to primary rim outward CD orientation, inverted triangle corresponds to secondary rim outward CD orientation and square corresponds edge-on CD orientation. Marks are numbered to identify each CD and track its mobility. Scale along the ϕ axis: 360° ≈ 23 nm at θ = 90°, for an arbitrary angle θ the scale increases as 23*sin(θ). Scale along the θ axis is constant: 180° ≈ 8.5 nm.

Although reduction in shell density resulted in significantly less core coverage and thinner shell, shell is still static with small changes in topographies and CD residues are almost equally distributed among possible orientations. As a result, only a small fraction of CD residues retain their functionality. These result indicate that CD orientation is an intrinsic property of a given combination of spacer and CDs and special measures should be taken to achieve a preferential secondary rim orientation of the CD. One of possible approaches may be use of a shorter and less flexible spacer and/or its covalent linkage to the primary rim of CDs at more than one point. Regarding the oligoglycine spacer used in this work, obtained results indicate that this spacer is convenient for creating static and stable scaffold consisting of a hydrophobic core and a thin shell decorated with functional CD residues, which will subsequently undergo further surface modifications by means of host-guest interactions to develop drug carriers with dynamic "stealth" shell, targeting ligands and diagnostic labels.

Conclusion

In present work we have studied arrangement and dynamics of α- and β-CDs decorating the surface of core-shell micelles with a shell formed by an oligoglycine spacer. It was found that CDs are distributed over the entire surface area, and are mostly located on the surface. However, due to their large surface density, most of CDs are found in clusters which adversely affects their ability to bind ligands. Moreover, CDs take various orientations, and only about 20% of them have their internal cavity exposed to the outside. Analysis of the dynamics of the surface structure of micelles showed that only a small part of the molecules retains mobility, which can also negatively affect their functionality. With a 5-fold decrease in the surface density of CDs and spacer, clusters of CD residues no longer formed, but however, the distribution of CD residues by orientation and their mobility remained without significant changes. Obtained results suggest that CDs orientation and mobility depend on combination of spacer, CD and their junctions and that special design efforts must be made to ensure CDs cavity exposure outside. Regarding combination of CDs and oligoglycine spacer used in this study, because of its tendency to form a stable static surface, it is suitable(after revision of CD-spacer junction, which will ensure proper orientation of the CDs) for development of scaffolds that can be easily functionalized by means of host-guest interactions to obtain functional drug delivery systems with required surface properties.

Acknowledgments

The work was carried out with the financial support of the Russian Science Foundation, grant No. 23-24-10046.

The calculations were carried out using a high-performance computing cluster of P.N. Lebedev Physical Institute of the Russian Academy of Sciences

Conflict of Interest

The authors declare no conflict of interest.

References:

1. Jain, Kewal K. "An overview of drug delivery systems." Drug delivery systems (2020): 1-54. doi: 10.1007/978-1-4939-9798-5_1
2. Wilhelm, Stefan, et al. "Analysis of nanoparticle delivery to tumours." *Nature reviews materials* 1.5 (2016): 1-12. https://doi.org/10.1038/natrevmats.2016.14
3. Rabanel, Jean-Michel, et al. "Nanoparticle heterogeneity: an emerging structural parameter influencing particle fate in biological media?." *Nanoscale* 11.2 (2019): 383-406. https://doi.org/10.1039/C8NR04916E

4. Mura, Simona, Julien Nicolas, and Patrick Couvreur. "Stimuli-responsive nanocarriers for drug delivery." *Nature materials* 12.11 (2013): 991-1003. https://doi.org/10.1038/nmat3776
5. Debayle, Manon, et al. "Zwitterionic polymer ligands: an ideal surface coating to totally suppress protein-nanoparticle corona formation?." *Biomaterials* 219 (2019): 119357. https://doi.org/10.1016/j.biomaterials.2019.119357
6. Schroffenegger, Martina, et al. "Polymer topology determines the formation of protein corona on core–shell nanoparticles." *ACS nano* 14.10 (2020): 12708-12718. https://doi.org/10.1021/acsnano.0c02358
7. Alberg, Irina, et al. "Polymeric nanoparticles with neglectable protein corona." *Small* 16.18 (2020): 1907574. https://doi.org/10.1002/smll.201907574
8. Manzari, Mandana T., et al. "Targeted drug delivery strategies for precision medicines." *Nature Reviews Materials* 6.4 (2021): 351-370. https://doi.org/10.1038/s41578-020-00269-6
9. Braga, Susana Santos. "Cyclodextrins: Emerging medicines of the new millennium." *Biomolecules* 9.12 (2019): 801. https://doi.org/10.3390/biom9120801
10. Carneiro, Simone Braga, et al. "Cyclodextrin–drug inclusion complexes: In vivo and in vitro approaches." *International journal of molecular sciences* 20.3 (2019): 642. https://doi.org/10.3390/ijms20030642
11. Devi, Lakshmi Sathi, et al. "Multifunctionality of cyclodextrin-based polymeric nanoparticulate delivery systems for chemotherapeutics, combination therapy, and theranostics." *International Journal of Pharmaceutics* (2024): 123976. https://doi.org/10.1016/j.ijpharm.2024.123976
12. Zhao, Yuqi, et al. "Engineered cyclodextrin-based supramolecular hydrogels for biomedical applications." *Journal of Materials Chemistry B* (2023). https://doi.org/10.1039/D3TB02101G
13. Utzeri, Gianluca, et al. "Cyclodextrin-based nanosponges: Overview and opportunities." *Frontiers in chemistry* 10 (2022): 859406. https://doi.org/10.3389/fchem.2022.859406
14. Rivero-Barbarroja, Gonzalo, et al. "Cyclodextrin-based functional glyconanomaterials." *Nanomaterials* 10.12 (2020): 2517. https://doi.org/10.3390/nano10122517
15. Łagiewka, Jakub, Tomasz Girek, and Wojciech Ciesielski. "Cyclodextrins-peptides/proteins conjugates: synthesis, properties and applications." *Polymers* 13.11 (2021): 1759. https://doi.org/10.3390/polym13111759
16. Xu, Chen, et al. "Versatile types of cyclodextrin-based nucleic acid delivery systems." *Advanced Healthcare Materials* 10.1 (2021): 2001183. https://doi.org/10.1002/adhm.202001183
17. Zhang, Ying-Ming, Yao-Hua Liu, and Yu Liu. "Cyclodextrin-based multistimuli-responsive supramolecular assemblies and their biological functions." *Advanced Materials* 32.3 (2020): 1806158. https://doi.org/10.1002/adma.201806158
18. Matencio, Adrián, et al. "Cyclodextrin monomers and polymers for drug activity enhancement." *Polymers* 13.11 (2021): 1684. https://doi.org/10.3390/polym13111684
19. Sharaf, Mehdi Ghaffari, et al. "Adsorption Dynamics of Uremic Toxins to Cyclodextrin-Coated Magnetic Nano-Adsorbents." *Carbohydrate Polymers* 347 (2025): 122573. https://doi.org/10.1016/j.carbpol.2024.122573
20. Soni, Shreya S., et al. "Uptake of Cyclodextrin Nanoparticles by Macrophages is Dependent on Particle Size and Receptor-Mediated Interactions." *ACS applied bio materials* (2024). https://doi.org/10.1021/acsabm.3c00985
21. Mayorga–Burrezo, Paula, et al. "Methamphetamine Removal from Aquatic Environments by Magnetic Microrobots with Cyclodextrin Chiral Recognition Elements." *Small* (2024): 2306943. https://doi.org/10.1002/smll.202306943
22. Nienhaus, Karin, and Gerd Ulrich Nienhaus. "Mechanistic understanding of protein Corona formation around nanoparticles: old puzzles and new insights." *Small* 19.28 (2023): 2301663. https://doi.org/10.1002/smll.202301663
23. Henry, Stephen, Williams, Eleanor, Barr, Katie, et al. "Rapid one-step biotinylation of biological and non-biological surfaces". *Scientific Reports*. 8, 2845 (2018). https://doi.org/10.1038/s41598-018-21186-3
24. Manalastas-Cantos, Karen, et al. "ATSAS 3.0: expanded functionality and new tools for small-angle scattering data analysis." *Journal of applied crystallography* 54.1 (2021): 343-355. https://doi.org/10.1107/S1600576720013412
25. Abraham, Mark James, et al. "GROMACS: High performance molecular simulations through multi-level parallelism from laptops to supercomputers." *SoftwareX* 1 (2015): 19-25. https://doi.org/10.1016/j.softx.2015.06.001
26. Stroet, Martin, et al. "Automated topology builder version 3.0: Prediction of solvation free enthalpies in water and hexane." *Journal of chemical theory and computation* 14.11 (2018): 5834-5845. https://doi.org/10.1021/acs.jctc.8b00768
27. Humphrey, William, Andrew Dalke, and Klaus Schulten. "VMD: visual molecular dynamics." *Journal of molecular graphics* 14.1 (1996): 33-38. https://doi.org/10.1016/0263-7855(96)00018-5
28. Svergun, D. I. B. C., Claudio Barberato, and Michel HJ Koch. "CRYSOL–a program to evaluate X-ray solution scattering of biological macromolecules from atomic coordinates." *Journal of applied crystallography* 28.6 (1995): 768-773. https://doi.org/10.1107/S0021889895007047
29. Vaskan, Ivan, et al. "Effect of ligand and shell densities on the surface structure of core–shell nanoparticles self-assembled from function–spacer–lipid constructs." *Biomaterials Science* 12.3 (2024): 798-806. https://doi.org/10.1039/D3BM01704D
30. Eisenhaber, Frank, et al. "The double cubic lattice method: Efficient approaches to numerical integration of surface area and volume and to dot surface contouring of molecular assemblies." *Journal of computational chemistry* 16.3 (1995): 273-284. https://doi.org/10.1002/jcc.540160303